

# Construction of rational surface patches bounded by lines of curvature

Luc Biard

Laboratoire Jean Kuntzmann,  
Université Joseph Fourier, Grenoble, FRANCE.

Rida T. Farouki

Department of Mechanical and Aeronautical Engineering,  
University of California, Davis, CA 95616, USA.

Nicolas Szafran

Laboratoire Jean Kuntzmann,  
Université Joseph Fourier, Grenoble, FRANCE.

## Abstract

The fact that the Darboux frame is rotation-minimizing along lines of curvature of a smooth surface is invoked to construct rational surface patches whose boundary curves are lines of curvature. For given patch corner points and associated frames defining the surface normals and principal directions, the patch boundaries are constructed as quintic RRMF curves, i.e., spatial Pythagorean-hodograph (PH) curves that possess rational rotation-minimizing frames. The interior of the patch is then defined as a Coons interpolant, matching the boundary curves and their associated rotation-minimizing frames as surface Darboux frames. The surface patches are compatible with the standard rational Bézier/B-spline representations, and  $G^1$  continuity between adjacent patches is easily achieved. Such patches are advantageous in surface design with more precise control over the surface curvature properties.

**Keywords:** Darboux frame; angular velocity; rotation-minimizing frame; lines of curvature; Pythagorean-hodograph curve; rational surface patch.  
e-mail: luc.biard@imag.fr, farouki@ucdavis.edu, nicolas.szafran@imag.fr

# 1 Introduction

As an extension of earlier studies [18, 19] concerned with constructing rational surface patches that have given geodesic boundary curves, we consider here the construction of patches with *lines of curvature* as boundary curves. The procedure exploits the fact that the Darboux frame is *rotation-minimizing* along surface lines of curvature, and the recent identification [11, 14] of curves that possess *rational rotation-minimizing frames* (RRMF curves).

By interpolating a set of RRMF curves as surface patch boundaries, with their associated rotation-minimizing frames describing the variation of the surface Darboux frame along them, one can construct rational surface patches whose boundary curves are automatically lines of curvature in a geometrically intuitive manner. This approach greatly extends the class of rational surface patches, bounded by lines of curvature, that can be constructed.

The first systematic investigation of surface patches bounded by lines of curvature was described in the PhD thesis [28] of R. R. Martin — who called them *principal patches*, since the tangents to the boundary curves correspond to *principal directions* on the surface — i.e., the orthogonal directions of the extremal *principal curvatures* at each point of a surface. Martin showed that the existence of such patches was contingent upon certain *position matching* and *frame matching* conditions along the patch boundary curves.

The construction of patches satisfying these conditions, from prescribed variations of the normal and geodesic curvatures along the boundaries, is a rather difficult process that does not ordinarily yield rational surface patches, although certain “simple” surfaces — such as generalized cylinders, surfaces of revolution, and the *Dupin cyclides* — permit easy construction of principal patches [28]. The Dupin cyclides (which are a special subclass of the rational biquadratic surfaces, and include the plane, cylinder, cone, sphere, and torus as special cases) are characterized by the fact that all their lines of curvature are simply circular arcs. However, the vertices of a four-sided Dupin cyclide principal patch are necessarily coplanar, a rather severe constraint in piecing them together for free-form surface design applications.

A different approach to constructing free-form surfaces bounded by lines of curvature is proposed herein, based on the observation that a space curve equipped with an *adapted orthonormal frame* (of which the curve tangent is one frame vector, and the other two span the curve normal plane) will be a line of curvature for any surface in which it is embedded, if one ensures that the frame is *rotation-minimizing* with respect to the curve tangent — i.e.,

its angular velocity vector has no component in the direction of the tangent. The ability to construct rational surfaces bounded by lines of curvature then follows from standard Coons interpolation schemes [4, 5, 7, 21].

Note that all RRMF curves must be *Pythagorean-hodograph* (PH) curves [10], since only PH curves possess rational unit tangent vectors. They may be characterized as proper subsets of the spatial PH curves by certain algebraic constraints on the coefficients of the quaternion and Hopf map representations [11, 14]. Actually, any spatial PH curve admits an essentially exact rotation-minimizing frame (RMF) computation, by integration of a rational function [9]. However, these RMFs do not ordinarily exhibit a rational dependence on the curve parameter, since rational functions do not in general have rational integrals. Thus, in order to obtain *rational* surface patches bounded by lines of curvature, we employ only RRMF curves as patch boundaries. A key step in the construction is the computation of RRMF curves interpolating given initial/final positions together with corresponding adapted frames.

The ability to construct rational patches (compatible with the standard Bézier/B-spline representations of contemporary CAD systems) bounded by lines of curvature is valuable in applications where smooth surfaces must be designed with more precise *a priori* control over surface curvature properties. For such patches, the normal curvature is extremal (with respect to direction) along the patch boundaries and orthogonal to them. Composite surfaces may thus be designed by laying out a grid of “feature lines” that are prescribed as lines of curvature, and using the procedures described below to construct the individual patches delineated by these feature lines. The patch construction scheme can easily ensure  $G^1$  continuity between adjacent patches, and may also be extended to accommodate  $G^2$  continuity.

The remainder of this paper is structured as follows. Section 2 reviews the relevant background on adapted frames, rotation-minimizing frames, PH curves, and the characterizations of RRMF curves and their construction as geometric Hermite interpolants. Concepts from surface differential geometry are then discussed in Section 3, including the Darboux frame, the principal curvatures/directions and lines of curvature, and the characterization of lines of curvature as loci along which the Darboux frame is rotation-minimizing. Section 4 then develops a construction for rational surface patches that match given RRMF boundary curves and their associated frames through a Coons interpolation scheme, and Section 5 presents computed examples of these rational patches bounded by lines of curvature. Finally, Section 6 summarizes key results of the paper, and identifies topics for further investigation.

## 2 Rational rotation–minimizing frame curves

Before proceeding to the problem of rational surface patches bounded by lines of curvature, we review below essential background information concerning rotation–minimizing adapted frames, PH curves, and RRMF curves.

### 2.1 Adapted frames on space curves

An *adapted frame*  $(\mathbf{t}, \mathbf{u}, \mathbf{v})$  on a space curve  $\mathbf{r}(\xi) = (x(\xi), y(\xi), z(\xi))$  is a set of three mutually orthogonal unit vectors, defined at each curve point, where  $\mathbf{t} = \mathbf{r}'/|\mathbf{r}'|$  is the curve tangent and  $\mathbf{u}, \mathbf{v}$  span the curve normal plane, such that  $\mathbf{u} \times \mathbf{v} = \mathbf{t}$ . The variation of such a frame may be defined in terms of its *angular velocity*  $\boldsymbol{\omega}(\xi)$ , through the differential relations

$$\frac{d\mathbf{t}}{d\xi} = \sigma \boldsymbol{\omega} \times \mathbf{t}, \quad \frac{d\mathbf{u}}{d\xi} = \sigma \boldsymbol{\omega} \times \mathbf{u}, \quad \frac{d\mathbf{v}}{d\xi} = \sigma \boldsymbol{\omega} \times \mathbf{v}, \quad (1)$$

where  $\sigma(\xi) = |\mathbf{r}'(\xi)|$  is the *parametric speed* of the curve  $\mathbf{r}(\xi)$ . The magnitude and direction of the angular velocity define the instantaneous angular speed  $\omega = |\boldsymbol{\omega}|$  and rotation axis  $\mathbf{a} = \boldsymbol{\omega}/|\boldsymbol{\omega}|$  of the adapted frame  $(\mathbf{t}, \mathbf{u}, \mathbf{v})$ .

There are infinitely many adapted frames on a given space curve  $\mathbf{r}(\xi)$  — if a particular adapted frame  $(\mathbf{t}, \mathbf{u}, \mathbf{v})$  is chosen as a reference, then for any scalar function  $\phi(\xi)$  another adapted frame can be defined [1] as

$$(\mathbf{t}, \cos \phi \mathbf{u} + \sin \phi \mathbf{v}, -\sin \phi \mathbf{u} + \cos \phi \mathbf{v}),$$

which corresponds to a rotation of the reference frame normal–plane vectors  $\mathbf{u}, \mathbf{v}$  through angle  $\phi(\xi)$  at each point of  $\mathbf{r}(\xi)$ .

Now since  $(\mathbf{t}, \mathbf{u}, \mathbf{v})$  comprise a basis for  $\mathbb{R}^3$  we can write

$$\boldsymbol{\omega} = \omega_1 \mathbf{t} + \omega_2 \mathbf{u} + \omega_3 \mathbf{v},$$

and hence we have

$$\frac{d\mathbf{t}}{d\xi} = \sigma(\omega_3 \mathbf{u} - \omega_2 \mathbf{v}), \quad \frac{d\mathbf{u}}{d\xi} = \sigma(\omega_1 \mathbf{v} - \omega_3 \mathbf{t}), \quad \frac{d\mathbf{v}}{d\xi} = \sigma(\omega_2 \mathbf{t} - \omega_1 \mathbf{u}).$$

The characteristic property of a *rotation–minimizing* adapted frame on  $\mathbf{r}(\xi)$  is that the component  $\omega_1$  of the angular velocity along  $\mathbf{t}$  vanishes identically, i.e.,  $\boldsymbol{\omega} \cdot \mathbf{t} \equiv 0$ . This implies that  $\mathbf{u}, \mathbf{v}$  have no instantaneous rotation about  $\mathbf{t}$ : they

vary only because  $\mathbf{t}$  varies along  $\mathbf{r}(\xi)$ , and they must remain orthogonal to it (and each other). Alternatively, the frame  $(\mathbf{t}, \mathbf{u}, \mathbf{v})$  is rotation–minimizing with respect to  $\mathbf{t}$  if the derivatives  $d\mathbf{u}/d\xi$ ,  $d\mathbf{v}/d\xi$  of the normal–plane vectors  $\mathbf{u}$ ,  $\mathbf{v}$  are always parallel to  $\mathbf{t}$ .

The most familiar adapted frame, the *Frenet frame*  $(\mathbf{t}, \mathbf{p}, \mathbf{b})$  defined by

$$\mathbf{t} = \frac{\mathbf{r}'}{|\mathbf{r}'|}, \quad \mathbf{p} = \frac{\mathbf{r}' \times \mathbf{r}''}{|\mathbf{r}' \times \mathbf{r}''|} \times \mathbf{t}, \quad \mathbf{b} = \frac{\mathbf{r}' \times \mathbf{r}''}{|\mathbf{r}' \times \mathbf{r}''|}, \quad (2)$$

describes [27] the *intrinsic geometry* of  $\mathbf{r}(\xi)$ . The *principal normal*  $\mathbf{p}$  points toward the *center of curvature*, while  $\mathbf{b} = \mathbf{t} \times \mathbf{p}$  is the *binormal*. The mutually orthogonal planes spanned by the vectors  $(\mathbf{t}, \mathbf{p})$ ,  $(\mathbf{p}, \mathbf{b})$ , and  $(\mathbf{b}, \mathbf{t})$  are called the *osculating*, *normal*, and *rectifying* planes at each point of  $\mathbf{r}(\xi)$ .

The angular velocity of the frame (2) is given [27] by the *Darboux vector*

$$\boldsymbol{\omega} = \kappa \mathbf{b} + \tau \mathbf{t}, \quad (3)$$

where the curvature  $\kappa$  and torsion  $\tau$  are defined by

$$\kappa = \frac{\mathbf{p} \cdot \mathbf{t}'}{\sigma} = \frac{|\mathbf{r}' \times \mathbf{r}''|}{|\mathbf{r}'|^3} \quad \text{and} \quad \tau = -\frac{\mathbf{p} \cdot \mathbf{b}'}{\sigma} = \frac{(\mathbf{r}' \times \mathbf{r}'') \cdot \mathbf{r}'''}{|\mathbf{r}' \times \mathbf{r}''|^2}.$$

With  $(\mathbf{u}, \mathbf{v}) = (\mathbf{p}, \mathbf{b})$  and  $\boldsymbol{\omega}$  given by (3), the relations (1) are equivalent to the well–known [27] *Frenet–Serret equations*

$$\begin{bmatrix} \mathbf{t}' \\ \mathbf{p}' \\ \mathbf{b}' \end{bmatrix} = \sigma \begin{bmatrix} 0 & \kappa & 0 \\ -\kappa & 0 & \tau \\ 0 & -\tau & 0 \end{bmatrix} \begin{bmatrix} \mathbf{t} \\ \mathbf{p} \\ \mathbf{b} \end{bmatrix}. \quad (4)$$

The magnitude  $|\boldsymbol{\omega}| = \sqrt{\kappa^2 + \tau^2}$  of the Darboux vector is also called the *total curvature* of the curve  $\mathbf{r}(\xi)$ . Note that, at points where  $\kappa = 0$ , the principal normal and binormal specified by (2) are indeterminate —  $\mathbf{p}$  and  $\mathbf{b}$  ordinarily suffer sudden reversals on traversing such *inflection points*.

## 2.2 Rotation–minimizing adapted frames

The Frenet frame (2) is *not* rotation–minimizing, since its angular velocity (3) contains the component  $\tau \mathbf{t}$ , which is non–zero for a non–planar curve. The

basis vectors  $(\mathbf{u}, \mathbf{v})$  of a rotation–minimizing frame (RMF) can be obtained from  $(\mathbf{p}, \mathbf{b})$  through a normal–plane rotation

$$\begin{bmatrix} \mathbf{u} \\ \mathbf{v} \end{bmatrix} = \begin{bmatrix} \cos \phi & \sin \phi \\ -\sin \phi & \cos \phi \end{bmatrix} \begin{bmatrix} \mathbf{p} \\ \mathbf{b} \end{bmatrix}, \quad (5)$$

defined by an suitable angle function  $\phi(\xi)$ . Klok [26] showed that the RMF basis vectors  $(\mathbf{u}, \mathbf{v})$  satisfy the differential equations

$$\mathbf{u}'(\xi) = -\frac{\mathbf{r}''(\xi) \cdot \mathbf{u}(\xi)}{\sigma^2(\xi)} \mathbf{r}'(\xi), \quad \mathbf{v}'(\xi) = -\frac{\mathbf{r}''(\xi) \cdot \mathbf{v}(\xi)}{\sigma^2(\xi)} \mathbf{r}'(\xi).$$

Substituting from (5), one can verify that these amount to the equation

$$\frac{d\phi}{d\xi} = -\sigma\tau = -|\mathbf{r}'| \frac{(\mathbf{r}' \times \mathbf{r}'') \cdot \mathbf{r}'''}{|\mathbf{r}' \times \mathbf{r}''|^2} \quad (6)$$

for the rotation angle  $\phi(\xi)$  used to obtain  $(\mathbf{u}, \mathbf{v})$  from  $(\mathbf{p}, \mathbf{b})$  in (5). Hence, as observed by Guggenheimer [22], this function has the form<sup>1</sup>

$$\phi(\xi) = \phi_0 - \int_0^\xi \tau(u) \sigma(u) du, \quad (7)$$

$\phi_0$  being an arbitrary integration constant. Thus, there are an infinite number of RMFs on a given space curve, corresponding to different values for  $\phi_0$ , but they differ from each other by only a fixed angular displacement  $\Delta\phi$  in the normal plane at each curve point. The essential difference between an RMF and the Frenet frame is that the former omits the term  $\tau \mathbf{t}$  from the Darboux vector (3), so its angular velocity is just  $\boldsymbol{\omega} = \kappa \mathbf{b}$ . The angular speed of an RMF is thus  $|\boldsymbol{\omega}| = \kappa$ , rather than  $|\boldsymbol{\omega}| = \sqrt{\kappa^2 + \tau^2}$  for the Frenet frame.

Since the integral in (7) does not ordinarily admit closed–form reduction for polynomial and rational curves, many schemes for the approximation of RMFs have been proposed [17, 23, 24, 25, 31, 32]. The spatial Pythagorean–hodograph (PH) curves are an exception [9] — for these curves the integrand reduces to a rational function, which may be integrated by a partial fraction decomposition (but this usually incurs transcendental terms).

---

<sup>1</sup>An incorrect sign before the integral is given in [22].

## 2.3 Pythagorean–hodograph curves

The *parametric speed* of a space curve  $\mathbf{r}(\xi) = (x(\xi), y(\xi), z(\xi))$  is the function

$$\sigma(\xi) = |\mathbf{r}'(\xi)| = \sqrt{x'^2(\xi) + y'^2(\xi) + z'^2(\xi)} \quad (8)$$

specifying the derivative  $ds/d\xi$  of arc length  $s$  with respect to the parameter  $\xi$ . Hence, arc length derivatives may be expressed as

$$\frac{d}{ds} = \frac{1}{\sigma(\xi)} \frac{d}{d\xi}.$$

A *Pythagorean–hodograph* (PH) *curve* is a polynomial curve characterized by the fact that its parametric speed is a *polynomial* in  $\xi$ . Hence, the hodograph (derivative)  $\mathbf{r}'(\xi) = (x'(\xi), y'(\xi), z'(\xi))$  components must satisfy

$$x'^2(\xi) + y'^2(\xi) + z'^2(\xi) \equiv \sigma^2(\xi) \quad (9)$$

for some polynomial  $\sigma(\xi)$ . A sufficient–and–necessary condition for satisfying the Pythagorean identity (9) is that  $x'(\xi)$ ,  $y'(\xi)$ ,  $z'(\xi)$ ,  $\sigma(\xi)$  are expressible [6] in terms of four polynomials  $u(\xi)$ ,  $v(\xi)$ ,  $p(\xi)$ ,  $q(\xi)$  in the form

$$\begin{aligned} x'(\xi) &= u^2(\xi) + v^2(\xi) - p^2(\xi) - q^2(\xi), \\ y'(\xi) &= 2[u(\xi)q(\xi) + v(\xi)p(\xi)], \\ z'(\xi) &= 2[v(\xi)q(\xi) - u(\xi)p(\xi)], \\ \sigma(\xi) &= u^2(\xi) + v^2(\xi) + p^2(\xi) + q^2(\xi). \end{aligned}$$

This structure is conveniently embodied in two algebraic models for spatial PH curves, introduced by Choi et al. [3]. In the *quaternion representation*, a Pythagorean hodograph is generated from a quaternion<sup>2</sup> polynomial  $\mathcal{A}(\xi) = u(\xi) + v(\xi)\mathbf{i} + p(\xi)\mathbf{j} + q(\xi)\mathbf{k}$  by the expression

$$\mathbf{r}'(\xi) = \mathcal{A}(\xi)\mathbf{i}\mathcal{A}^*(\xi), \quad (10)$$

$\mathcal{A}^*(\xi) = u(\xi) - v(\xi)\mathbf{i} - p(\xi)\mathbf{j} - q(\xi)\mathbf{k}$  being the conjugate of  $\mathcal{A}(\xi)$ . Note that the expression on the right in (10) is a quaternion with zero scalar part — i.e., a vector in  $\mathbb{R}^3$ . The *Hopf map representation*, on the other hand, generates a

---

<sup>2</sup>Calligraphic characters denote quaternions, the scalar and vector components [29] of a quaternion  $\mathcal{A}$  being indicated by  $\text{scal}(\mathcal{A})$  and  $\text{vect}(\mathcal{A})$ . When pure scalars or vectors are juxtaposed with quaternions, the quaternion product is imputed.

Pythagorean hodograph from two complex polynomials<sup>3</sup>  $\boldsymbol{\alpha}(\xi) = u(\xi) + i v(\xi)$ ,  $\boldsymbol{\beta}(\xi) = q(\xi) + i p(\xi)$  through the expression

$$\mathbf{r}'(\xi) = (|\boldsymbol{\alpha}(\xi)|^2 - |\boldsymbol{\beta}(\xi)|^2, 2 \operatorname{Re}(\boldsymbol{\alpha}(\xi)\overline{\boldsymbol{\beta}(\xi)}), 2 \operatorname{Im}(\boldsymbol{\alpha}(\xi)\overline{\boldsymbol{\beta}(\xi)})). \quad (11)$$

The equivalence of (10) and (11) may be seen by taking  $\mathcal{A}(\xi) = \boldsymbol{\alpha}(\xi) + \mathbf{k} \boldsymbol{\beta}(\xi)$ , the imaginary unit  $i$  being identified with the quaternion basis element  $\mathbf{i}$ .

## 2.4 Rational rotation–minimizing frames

The possibility of constructing polynomial curves that have *rational rotation–minimizing frames* (RRMF curves) has recently been demonstrated — these are necessarily PH curves, since only PH curves have rational unit tangents. Hence, RRMF curves can be characterized by identifying constraints on the coefficients of PH curves that are sufficient and necessary for the existence of a rational RMF. In this context, the Frenet frame (2) is not a good reference for identifying rational RMFs, because it is inherently non–rational and can exhibit singular behavior ( $\mathbf{p}$  and  $\mathbf{b}$  suddenly reverse) at inflections.

To remedy these problems, Choi and Han [2] identified a rational adapted frame on spatial PH curves, the *Euler–Rodrigues frame* (ERF), defined by

$$\mathbf{t} = \frac{\mathcal{A}(\xi) \mathbf{i} \mathcal{A}^*(\xi)}{|\mathcal{A}(\xi)|^2}, \quad \mathbf{f} = \frac{\mathcal{A}(\xi) \mathbf{j} \mathcal{A}^*(\xi)}{|\mathcal{A}(\xi)|^2}, \quad \mathbf{g} = \frac{\mathcal{A}(\xi) \mathbf{k} \mathcal{A}^*(\xi)}{|\mathcal{A}(\xi)|^2}.$$

This frame is not intrinsic (it depends upon the chosen coordinate system) — but it is always rational and non–singular. Han [20] subsequently identified an algebraic criterion characterizing RRMF curves. Namely, the hodograph (10) defines an RRMF curve if and only if two relatively prime polynomials  $a(\xi)$ ,  $b(\xi)$  exist, such that the components  $u(\xi)$ ,  $v(\xi)$ ,  $p(\xi)$ ,  $q(\xi)$  of  $\mathcal{A}(\xi)$  satisfy

$$\frac{uv' - u'v - pq' + p'q}{u^2 + v^2 + p^2 + q^2} = \frac{ab' - a'b}{a^2 + b^2}. \quad (12)$$

If this is satisfied, the RMF  $(\mathbf{t}, \mathbf{u}, \mathbf{v})$  can be obtained from the ERF  $(\mathbf{t}, \mathbf{f}, \mathbf{g})$  through the rational rotation specified by

$$\mathbf{u} = \frac{a^2 - b^2}{a^2 + b^2} \mathbf{f} - \frac{2ab}{a^2 + b^2} \mathbf{g}, \quad \mathbf{v} = \frac{2ab}{a^2 + b^2} \mathbf{f} + \frac{a^2 - b^2}{a^2 + b^2} \mathbf{g}. \quad (13)$$

---

<sup>3</sup>Bold font symbols are used to denote both complex numbers and vectors in  $\mathbb{R}^3$  — the meaning should be clear from the context.

It was shown in [20] that all RRMF cubics are degenerate (i.e., planar curves, or curves with non-primitive hodographs). The existence of non-degenerate RRMF quintics was first constructively demonstrated in [14], in which they were identified by one real and one complex constraint on the six complex coefficients that specify the Hopf map form of spatial PH quintics. A much simpler (and more symmetric) characterization of these RRMF quintics was subsequently derived in [11], including a formulation in terms of the more commonly-used quaternion representation of spatial PH curves.

The following propositions state the key results concerning identification of quintic RRMF curves in the quaternion and Hopf map representations of spatial PH curves — see [11] for complete details and proofs.

**Proposition 1.** *A spatial PH quintic specified in the quaternion form (10) by the quadratic quaternion polynomial*

$$\mathcal{A}(\xi) = \mathcal{A}_0(1 - \xi)^2 + \mathcal{A}_1 2(1 - \xi)\xi + \mathcal{A}_2 \xi^2 \quad (14)$$

*has a rational RMF if and only if the coefficients of this polynomial satisfy*

$$\text{vect}(\mathcal{A}_2 \mathbf{i} \mathcal{A}_0^*) = \mathcal{A}_1 \mathbf{i} \mathcal{A}_1^*. \quad (15)$$

**Proposition 2.** *A spatial PH quintic specified in the Hopf map form (11) by quadratic complex polynomials*

$$\begin{aligned} \boldsymbol{\alpha}(\xi) &= \boldsymbol{\alpha}_0 (1 - \xi)^2 + \boldsymbol{\alpha}_1 2(1 - \xi)\xi + \boldsymbol{\alpha}_2 \xi^2, \\ \boldsymbol{\beta}(\xi) &= \boldsymbol{\beta}_0 (1 - \xi)^2 + \boldsymbol{\beta}_1 2(1 - \xi)\xi + \boldsymbol{\beta}_2 \xi^2, \end{aligned} \quad (16)$$

*has a rational RMF if and only if the coefficients of these polynomials satisfy*

$$\text{Re}(\boldsymbol{\alpha}_0 \bar{\boldsymbol{\alpha}}_2 - \boldsymbol{\beta}_0 \bar{\boldsymbol{\beta}}_2) = |\boldsymbol{\alpha}_1|^2 - |\boldsymbol{\beta}_1|^2, \quad \boldsymbol{\alpha}_0 \bar{\boldsymbol{\beta}}_2 + \boldsymbol{\alpha}_2 \bar{\boldsymbol{\beta}}_0 = 2 \boldsymbol{\alpha}_1 \bar{\boldsymbol{\beta}}_1. \quad (17)$$

## 2.5 Geometric Hermite interpolation

In order to employ quintic RRMF curves as surface patch boundaries that are lines of curvature, it is necessary to have algorithms for geometric design with these curves. In the standard  $C^1$  Hermite interpolation algorithm [12, 13] for spatial PH quintics, there are two residual scalar freedoms. The conditions (15) or (17) that identify the RRMF quintics among all spatial PH quintics amount to three scalar constraints. Hence, by relaxing from  $C^1$  to  $G^1$  data,

it should be possible to construct RRMF quintic interpolants to specified end points and (unit) tangents, with one residual scalar freedom.

A preliminary study of  $G^1$  Hermite interpolation by RRMF quintics was presented in [16], and a more complete analysis was subsequently described in [15]. To embed an RRMF quintic as a surface line of curvature, its RMF must coincide with the surface Darboux frame (see Section 3.1 below). Since computing RMFs is an initial value problem, the surface normal at one end of an RRMF quintic intended as a line-of-curvature patch boundary can be freely chosen. The residual scalar freedom must then be used in matching the desired surface normal at the other end, i.e., the curve must interpolate given end points *and* its RMF must interpolate given end frames. Because of the highly non-linear nature of this problem [15], it has not been possible to verify the existence of RRMF quintic interpolants to arbitrary end points/frames. It should be possible to remedy this by introducing more degrees of freedom. For example, the hodograph of an RRMF quintic can be multiplied by a scalar polynomial, without compromising its rational RMF property. Alternatively, one may appeal to RRMF curves of degree 7 or more.

### 3 Lines of curvature on a surface

For a curve on a smooth surface, the Darboux frame  $(\mathbf{t}, \mathbf{h}, \mathbf{n})$  is an adapted frame incorporating the *surface normal*  $\mathbf{n}$  as one of the two vectors that span the curve normal plane at each point. The other vector  $\mathbf{h} = \mathbf{n} \times \mathbf{t}$  is called the *tangent normal*, since it lies in the surface *tangent plane* and is orthogonal to the curve tangent  $\mathbf{t}$  at each point. It is shown below that the Darboux frame is rotation-minimizing along a curve on a smooth surface if and only if the curve is a line of curvature. We now review the necessary ideas from surface differential geometry that allow the RRMF curves to be used in constructing rational patches bounded by lines of curvature.

#### 3.1 Darboux frame on a surface curve

Consider a curve  $\mathbf{r}(\xi) = \mathbf{s}(u(\xi), v(\xi))$  on the surface  $\mathbf{s}(u, v)$ , specified by the parameter functions  $u(\xi), v(\xi)$ . Denoting the surface partial derivatives by  $\mathbf{s}_u$  and  $\mathbf{s}_v$ , the *Darboux frame*  $(\mathbf{t}, \mathbf{h}, \mathbf{n})$  along this curve is defined by

$$\mathbf{t} = \frac{u' \mathbf{s}_u + v' \mathbf{s}_v}{|u' \mathbf{s}_u + v' \mathbf{s}_v|}, \quad \mathbf{h} = \frac{\mathbf{s}_u \times \mathbf{s}_v}{|\mathbf{s}_u \times \mathbf{s}_v|} \times \mathbf{t}, \quad \mathbf{n} = \frac{\mathbf{s}_u \times \mathbf{s}_v}{|\mathbf{s}_u \times \mathbf{s}_v|}, \quad (18)$$

where  $\mathbf{t}$  is the *tangent* to the curve  $\mathbf{r}(\xi)$ ,  $\mathbf{n}$  is the *surface normal* along  $\mathbf{r}(\xi)$ , and the vector  $\mathbf{h} = \mathbf{n} \times \mathbf{t}$  is called the *tangent normal*.

The variation of the Darboux frame along the curve  $\mathbf{r}(\xi) = \mathbf{s}(u(\xi), v(\xi))$  is described [27, 30] by the equations

$$\begin{bmatrix} \mathbf{t}' \\ \mathbf{h}' \\ \mathbf{n}' \end{bmatrix} = \sigma \begin{bmatrix} 0 & \kappa_g & \kappa_n \\ -\kappa_g & 0 & -\tau_g \\ -\kappa_n & \tau_g & 0 \end{bmatrix} \begin{bmatrix} \mathbf{t} \\ \mathbf{h} \\ \mathbf{n} \end{bmatrix}, \quad (19)$$

where

$$\sigma = |u'\mathbf{s}_u + v'\mathbf{s}_v|, \quad \kappa_n = \frac{\mathbf{n} \cdot \mathbf{t}'}{\sigma}, \quad \kappa_g = \frac{\mathbf{h} \cdot \mathbf{t}'}{\sigma}, \quad \tau_g = \frac{\mathbf{h} \cdot \mathbf{n}'}{\sigma}$$

are the parametric speed, *normal curvature*, and the *geodesic curvature* and *geodesic torsion* of  $\mathbf{r}(\xi)$ . Geodesic curvature measures the deviation between the principal normal  $\mathbf{p}$  of the curve and the surface normal  $\mathbf{n}$  along it — a geodesic curve is characterized by the fact that  $\mathbf{p} \equiv \mathbf{n}$ , and hence  $\kappa_g \equiv 0$ . The geodesic torsion in any chosen direction at a given surface point is the torsion of the geodesic in the chosen direction at that point. For a geodesic curve, the geodesic torsion is thus identical to the “ordinary” torsion,  $\tau_g \equiv \tau$ . From (19) we see that the angular velocity of the Darboux frame is

$$\boldsymbol{\omega} = -\tau_g \mathbf{t} - \kappa_n \mathbf{h} + \kappa_g \mathbf{n}. \quad (20)$$

The *lines of curvature* on a surface satisfy  $\tau_g \equiv 0$  [27].

To understand the rotation–minimizing property of the Darboux frame along lines of curvature, we need to review some basic surface geometry [27]. The *normal curvature* along  $\mathbf{r}(\xi) = \mathbf{s}(u(\xi), v(\xi))$  is defined by

$$\kappa_n = - \frac{Lu'^2 + 2Mu'v' + Nv'^2}{Eu'^2 + 2Fu'v' + Gv'^2}, \quad (21)$$

where the coefficients of the first and second fundamental forms are

$$E = \mathbf{s}_u \cdot \mathbf{s}_u, \quad F = \mathbf{s}_u \cdot \mathbf{s}_v, \quad G = \mathbf{s}_v \cdot \mathbf{s}_v, \quad (22)$$

$$L = \mathbf{n} \cdot \mathbf{s}_{uu}, \quad M = \mathbf{n} \cdot \mathbf{s}_{uv}, \quad N = \mathbf{n} \cdot \mathbf{s}_{vv}. \quad (23)$$

At each point of  $\mathbf{r}(\xi) = \mathbf{s}(u(\xi), v(\xi))$  expression (21) gives the curvature of the section of the surface by the plane spanned by the vectors  $\mathbf{t}$ ,  $\mathbf{n}$  at that point. At any point of  $\mathbf{s}(u, v)$  the normal curvature  $\kappa$  may be considered as a

function of the ratio  $u' : v'$  that defines the orientation  $\mathbf{t}$  of the section plane about the surface normal  $\mathbf{n}$ . The extrema of (21) with respect to this ratio, the *principal curvatures* at the point under consideration, are given by

$$\kappa_{\min} = H - \sqrt{H^2 - K} \quad \text{and} \quad \kappa_{\max} = H + \sqrt{H^2 - K}, \quad (24)$$

where the *mean curvature*  $H = \frac{1}{2}(\kappa_{\min} + \kappa_{\max})$  and *Gaussian curvature*  $K = \kappa_{\min}\kappa_{\max}$  are defined at each surface point by

$$H = \frac{2FM - EN - GL}{2(EG - F^2)} \quad \text{and} \quad K = \frac{LN - M^2}{EG - F^2}. \quad (25)$$

The Gaussian, mean, and principal curvatures are *intrinsic* properties, i.e., they are invariant under any (proper) re-parameterization of the surface.

The directions in which the principal curvatures are attained — i.e., the *principal directions* of the surface at each point — are given by the ratios

$$u' : v' = -(\kappa_p F + M) : \kappa_p E + L = -(\kappa_p G + N) : \kappa_p F + M, \quad (26)$$

with  $\kappa_p = \kappa_{\min}$  or  $\kappa_{\max}$ . These two principal directions are always orthogonal. Exceptionally, the two principal directions are indeterminate at surface points where  $E : F : G = L : M : N$ , so that  $H^2 = K$  and  $\kappa_{\min} = \kappa_{\max}$ , since the normal curvature is then *independent of direction* — the surface is of spherical shape in the neighborhood of such *umbilic* points.

The *lines of curvature* on a surface are two families of curves, each tangent to one of the principal directions at every point, forming an “orthogonal net” that covers the surface. Choosing the first of equations (26), we obtain the system of first-order differential equations

$$\frac{du}{dt} = -\alpha(\kappa_p F + M) \quad \text{and} \quad \frac{dv}{dt} = \alpha(\kappa_p E + L), \quad (27)$$

where the function  $\alpha$  determines the *parameterization* of the line of curvature. If we choose arc length  $s$  along a line of curvature for the parameter  $t$ , this function is given by

$$\alpha = \frac{\pm 1}{\sqrt{E(\kappa_p F + M)^2 - 2F(\kappa_p F + M)(\kappa_p E + L) + G(\kappa_p E + L)^2}},$$

where the chosen sign fixes the sense in which  $s$  increases. Alternatively, the other ratio in (26) can be used to obtain the system

$$\frac{du}{dt} = -\beta(\kappa_p G + N) \quad \text{and} \quad \frac{dv}{dt} = \beta(\kappa_p F + M), \quad (28)$$

where, for  $t = s$ , we now have

$$\beta = \frac{\pm 1}{\sqrt{E(\kappa_p G + N)^2 - 2F(\kappa_p G + N)(\kappa_p F + M) + G(\kappa_p F + M)^2}}.$$

It may be necessary to switch between (27) and (28) when *both* right-hand sides in one system vanish [8]: this occurs when a principal direction coincides with one surface parameter direction. Of course, neither of these systems can be integrated at an umbilic point. In (27) and (28),  $\kappa_p$  is consistently set to  $\kappa_{\min}$  or  $\kappa_{\max}$  — these choices yield lines of “minimum” and “maximum” curvature. Since the differential equations are first order, computing lines of curvature is an *initial value problem*. A unique pair of lines of curvature pass orthogonally through any chosen (non-umbilic) point.

From the angular velocity (20) of the Darboux frame, we see that it is rotation-minimizing along a given curve if and only if the geodesic torsion vanishes along that path. We can directly verify that such paths correspond to the *lines of curvature* of the surface as follows.

**Proposition 3.** *The Darboux frame is rotation-minimizing along the lines of curvature of a surface  $\mathbf{s}(u, v)$ .*

*Proof.* In order for the frame (18) to be rotation-minimizing, the derivative of the surface normal  $\mathbf{n}$  must be proportional to the tangent  $\mathbf{t}$  — i.e., there must be a scalar function  $\lambda(\xi)$  such that

$$\frac{u'\mathbf{s}_u + v'\mathbf{s}_v}{|u'\mathbf{s}_u + v'\mathbf{s}_v|} = \lambda \frac{d}{d\xi} \frac{\mathbf{s}_u \times \mathbf{s}_v}{|\mathbf{s}_u \times \mathbf{s}_v|}.$$

Expanding the derivative and taking dot products with  $\mathbf{s}_u$  and  $\mathbf{s}_v$ , we obtain

$$\begin{aligned} \frac{u'(\mathbf{s}_u \cdot \mathbf{s}_u) + v'(\mathbf{s}_u \cdot \mathbf{s}_v)}{|u'\mathbf{s}_u + v'\mathbf{s}_v|} &= \lambda \frac{[(u'\mathbf{s}_{uu} + v'\mathbf{s}_{uv}) \times \mathbf{s}_v] \cdot \mathbf{s}_u}{|\mathbf{s}_u \times \mathbf{s}_v|}, \\ \frac{u'(\mathbf{s}_u \cdot \mathbf{s}_v) + v'(\mathbf{s}_v \cdot \mathbf{s}_v)}{|u'\mathbf{s}_u + v'\mathbf{s}_v|} &= \lambda \frac{[\mathbf{s}_u \times (u'\mathbf{s}_{uv} + v'\mathbf{s}_{vv})] \cdot \mathbf{s}_v}{|\mathbf{s}_u \times \mathbf{s}_v|}. \end{aligned}$$

Now  $|u'\mathbf{s}_u + v'\mathbf{s}_v|$  is the parametric speed  $\sigma$  of the curve  $\mathbf{r}(\xi) = \mathbf{s}(u(\xi), v(\xi))$ , and the coefficients of  $u'$ ,  $v'$  on the left are the quantities (22). Similarly, re-arranging the triple products allows us to write the coefficients of  $u'$ ,  $v'$  on the right in terms of the quantities (23). Simplification then yields the homogeneous linear differential equations

$$\begin{bmatrix} E + \lambda \sigma L & F + \lambda \sigma M \\ F + \lambda \sigma M & G + \lambda \sigma N \end{bmatrix} \begin{bmatrix} u' \\ v' \end{bmatrix} = \begin{bmatrix} 0 \\ 0 \end{bmatrix} \quad (29)$$

for  $u', v'$ . To be consistent, the determinant of the above matrix must vanish, and this yields the quadratic equation

$$(LN - M^2) \lambda^2 \sigma^2 + (EN + GL - 2FM) \lambda \sigma + EG - F^2 = 0$$

in  $\lambda \sigma$ , with roots expressible in terms of the mean and Gaussian curvatures (25) — or equivalently the principal curvatures (24) — as

$$\lambda \sigma = \frac{H \pm \sqrt{H^2 - K}}{K} = \frac{1}{\kappa_p},$$

where  $\kappa_p = \kappa_{\min}$  or  $\kappa_{\max}$ . Hence, the frame  $(\mathbf{t}, \mathbf{h}, \mathbf{n})$  is rotation–minimizing along those paths on the surface for which equations (29) coincide with the conditions (26) that characterize its lines of curvature. ■

Of course, the lines of curvature defined by integrating (27) or (28) on a free–form polynomial or rational surfaces are not ordinarily polynomial or rational curves — the ability to construct rational surfaces with polynomial boundary curves as lines of curvature is therefore quite extraordinary.

## 4 Lines of curvature as patch boundaries

An RRMF curve  $\mathbf{r}(\xi)$  with associated rational rotation–minimizing adapted frame  $(\mathbf{t}(\xi), \mathbf{u}(\xi), \mathbf{v}(\xi))$  can be incorporated as one boundary of a rational surface patch, that is also a line of curvature, if the surface is constructed so that the rotation–minimizing frame coincides with the Darboux frame on  $\mathbf{r}(\xi)$ . By geometric Hermite interpolation with RRMF curves, suitable curves  $\mathbf{r}(\xi)$  and RMFs  $(\mathbf{t}(\xi), \mathbf{u}(\xi), \mathbf{v}(\xi))$  can be constructed [15] matching given end points  $\mathbf{r}(0)$  and  $\mathbf{r}(1)$  and frames  $(\mathbf{t}(0), \mathbf{u}(0), \mathbf{v}(0))$  and  $(\mathbf{t}(1), \mathbf{u}(1), \mathbf{v}(1))$ .

### 4.1 Construction of 4–sided patches

The initial data consists of the four patch corner points  $\mathbf{p}_{ij}$  and corresponding orthonormal frames  $(\mathbf{t}_{ij}, \mathbf{h}_{ij}, \mathbf{n}_{ij})$  identifying the surface principal directions and normals for  $i, j = 0, 1$ . The first step is to construct RRMF curves  $\mathbf{r}_k(\xi)$ ,

$k = 1, \dots, 4$  defining a curvilinear rectangle (see Figure 1), such that

$$\begin{aligned}
\mathbf{r}_1(0) &= \mathbf{p}_{00}, & \mathbf{r}_1(1) &= \mathbf{p}_{10}, \\
\mathbf{r}_2(0) &= \mathbf{p}_{00}, & \mathbf{r}_2(1) &= \mathbf{p}_{01}, \\
\mathbf{r}_3(0) &= \mathbf{p}_{01}, & \mathbf{r}_3(1) &= \mathbf{p}_{11}, \\
\mathbf{r}_4(0) &= \mathbf{p}_{10}, & \mathbf{r}_4(1) &= \mathbf{p}_{11}.
\end{aligned} \tag{30}$$

Also, the rational rotation–minimizing adapted frames associated with these curves, denoted by  $(\mathbf{t}_k(\xi), \mathbf{h}_k(\xi), \mathbf{n}_k(\xi))$  where  $\mathbf{t}_k(\xi) = \mathbf{r}'_k(\xi)/|\mathbf{r}'_k(\xi)|$ , are to be identified with the surface Darboux frames along each boundary curve  $\mathbf{r}_k(\xi)$ , as in Figure 1. Noting that the lines of curvature are orthogonal at each point, the initial and final frames  $(\mathbf{t}_k(0), \mathbf{h}_k(0), \mathbf{n}_k(0))$  and  $(\mathbf{t}_k(1), \mathbf{h}_k(1), \mathbf{n}_k(1))$  for each curve  $\mathbf{r}_k(\xi)$  must satisfy

$$\begin{aligned}
(\mathbf{t}_1(0), \mathbf{h}_1(0), \mathbf{n}_1(0)) &= (\mathbf{t}_{00}, \mathbf{h}_{00}, \mathbf{n}_{00}), \\
(\mathbf{t}_1(1), \mathbf{h}_1(1), \mathbf{n}_1(1)) &= (\mathbf{t}_{10}, \mathbf{h}_{10}, \mathbf{n}_{10}), \\
(\mathbf{t}_2(0), \mathbf{h}_2(0), \mathbf{n}_2(0)) &= (\mathbf{h}_{00}, -\mathbf{t}_{00}, \mathbf{n}_{00}), \\
(\mathbf{t}_2(1), \mathbf{h}_2(1), \mathbf{n}_2(1)) &= (\mathbf{h}_{01}, -\mathbf{t}_{01}, \mathbf{n}_{01}), \\
(\mathbf{t}_3(0), \mathbf{h}_3(0), \mathbf{n}_3(0)) &= (\mathbf{t}_{01}, \mathbf{h}_{01}, \mathbf{n}_{01}), \\
(\mathbf{t}_3(1), \mathbf{h}_3(1), \mathbf{n}_3(1)) &= (\mathbf{t}_{11}, \mathbf{h}_{11}, \mathbf{n}_{11}), \\
(\mathbf{t}_4(0), \mathbf{h}_4(0), \mathbf{n}_4(0)) &= (\mathbf{h}_{10}, -\mathbf{t}_{10}, \mathbf{n}_{10}), \\
(\mathbf{t}_4(1), \mathbf{h}_4(1), \mathbf{n}_4(1)) &= (\mathbf{h}_{11}, -\mathbf{t}_{11}, \mathbf{n}_{11}).
\end{aligned} \tag{31}$$

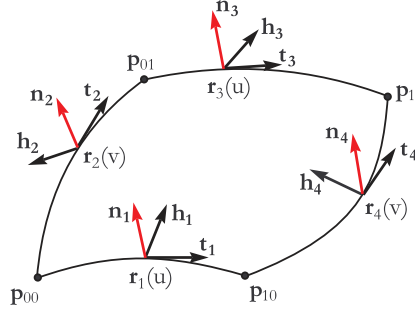


Figure 1: Orientation of Darboux frames (RMFs) along patch boundaries.

The four boundary curves  $\mathbf{r}_k(\xi)$ ,  $k = 1, \dots, 4$  are constructed as RRMF quintic interpolants to the end points and end frames, defined in terms of

the initial data by (30) and (31). If we construct a surface patch bounded by these curves, such that their rotation–minimizing frames coincide with the Darboux frame, the geodesic torsion will vanish along them, and they will be lines of curvature on the surface.

The construction of the interpolating surface  $\mathbf{s}(u, v)$  will ensure that the four boundary curves  $\mathbf{r}_1(\xi)$ ,  $\mathbf{r}_2(\xi)$ ,  $\mathbf{r}_3(\xi)$ ,  $\mathbf{r}_4(\xi)$  correspond, respectively, to the surface isoparametric curves  $\mathbf{s}(u, 0)$ ,  $\mathbf{s}(0, v)$ ,  $\mathbf{s}(u, 1)$ ,  $\mathbf{s}(1, v)$ . Furthermore, for each fixed value  $u_*$  and  $v_*$  of  $u$  and  $v$ , the two families of isoparametric curves  $\mathbf{s}(u, v_*)$  and  $\mathbf{s}(u_*, v)$  will meet the “boundary lines of curvature” orthogonally — i.e., in the complementary principal direction.

## 4.2 Coons interpolation scheme

In addition to the four boundary curves  $\mathbf{r}_k(\xi)$ ,  $k = 1, \dots, 4$  the cubic Coons interpolation scheme requires a field of “departure/arrival” vectors  $\mathbf{T}_k(\xi)$  to be defined in the surface tangent plane along each curve. These vectors have the general form

$$\mathbf{T}_k(\xi) = x_k(\xi) \mathbf{t}_k(\xi) + y_k(\xi) \mathbf{h}_k(\xi), \quad k = 1, \dots, 4, \quad (32)$$

where  $x_k(\xi)$  and  $y_k(\xi)$  are polynomial functions, defined below. As in [18, 19] the vector fields  $\mathbf{T}_k(\xi)$  must satisfy the following conditions.

- Interpolation of the corner derivatives (Section 4.3.1):

$$\mathbf{T}_1(0) = \mathbf{r}'_2(0) \quad \text{and} \quad \mathbf{T}_1(1) = \mathbf{r}'_4(0), \quad (33)$$

$$\mathbf{T}_2(0) = \mathbf{r}'_1(0) \quad \text{and} \quad \mathbf{T}_2(1) = \mathbf{r}'_3(0), \quad (34)$$

$$\mathbf{T}_3(0) = \mathbf{r}'_2(1) \quad \text{and} \quad \mathbf{T}_3(1) = \mathbf{r}'_4(1), \quad (35)$$

$$\mathbf{T}_4(0) = \mathbf{r}'_1(1) \quad \text{and} \quad \mathbf{T}_4(1) = \mathbf{r}'_3(1), \quad (36)$$

— i.e., the vectors (32) must coincide with the end derivatives of the two curves meeting at each of the four surface patch corners.

- Twist vector constraints at the patch corners (Section 4.3.2) — the vector fields  $\mathbf{T}_k(\xi)$  must satisfy the following compatibility constraints,

from which the twist vectors  $\mathbf{s}_{uv}(i, j)$  for  $i, j = 0, 1$  are deduced:

$$\left. \frac{d}{du} \mathbf{T}_1(u) \right|_{u=0} = \left. \frac{d}{dv} \mathbf{T}_2(v) \right|_{v=0} =: \mathbf{s}_{uv}(0, 0), \quad (37)$$

$$\left. \frac{d}{dv} \mathbf{T}_2(v) \right|_{v=1} = \left. \frac{d}{du} \mathbf{T}_3(u) \right|_{u=0} =: \mathbf{s}_{uv}(0, 1), \quad (38)$$

$$\left. \frac{d}{du} \mathbf{T}_3(u) \right|_{u=1} = \left. \frac{d}{dv} \mathbf{T}_4(v) \right|_{v=1} =: \mathbf{s}_{uv}(1, 1), \quad (39)$$

$$\left. \frac{d}{dv} \mathbf{T}_4(v) \right|_{v=0} = \left. \frac{d}{du} \mathbf{T}_1(u) \right|_{u=1} =: \mathbf{s}_{uv}(1, 0). \quad (40)$$

### 4.3 Cubic Coons interpolant

Consider the three surfaces  $\mathbf{s}_{13}(u, v)$ ,  $\mathbf{s}_{24}(u, v)$ ,  $\mathbf{s}_0(u, v)$  defined by

$$\mathbf{s}_{13}(u, v) = [C_0(v) \ C_1(v) \ C_2(v) \ C_3(v)] \begin{bmatrix} \mathbf{r}_1(u) \\ \mathbf{T}_1(u) \\ \mathbf{T}_3(u) \\ \mathbf{r}_3(u) \end{bmatrix},$$

$$\mathbf{s}_{24}(u, v) = [C_0(u) \ C_1(u) \ C_2(u) \ C_3(u)] \begin{bmatrix} \mathbf{r}_2(v) \\ \mathbf{T}_2(v) \\ \mathbf{T}_4(v) \\ \mathbf{r}_4(v) \end{bmatrix},$$

$$\mathbf{s}_0(u, v) =$$

$$[C_0(u) \ C_1(u) \ C_2(u) \ C_3(u)] \begin{bmatrix} \mathbf{p}_{00} & \mathbf{r}'_2(0) & \mathbf{r}'_2(1) & \mathbf{p}_{01} \\ \mathbf{r}'_1(0) & \mathbf{s}_{uv}(0, 0) & \mathbf{s}_{uv}(0, 1) & \mathbf{r}'_3(0) \\ \mathbf{r}'_1(1) & \mathbf{s}_{uv}(1, 0) & \mathbf{s}_{uv}(1, 1) & \mathbf{r}'_3(1) \\ \mathbf{p}_{10} & \mathbf{r}'_4(0) & \mathbf{r}'_4(1) & \mathbf{p}_{11} \end{bmatrix} \begin{bmatrix} C_0(v) \\ C_1(v) \\ C_2(v) \\ C_3(v) \end{bmatrix}$$

where  $C_0(\xi), \dots, C_3(\xi)$  are the cubic Hermite basis functions (see Appendix). The desired interpolating surface is then defined by

$$\mathbf{s}(u, v) = \mathbf{s}_{13}(u, v) + \mathbf{s}_{24}(u, v) - \mathbf{s}_0(u, v). \quad (41)$$

### 4.3.1 Interpolation of corner derivatives

To satisfy the conditions (31) and (33–36), we must choose  $x_k(0) = x_k(1) = 0$  for  $k = 1, \dots, 4$  in the general form (32) of the departure/arrival vectors  $\mathbf{T}_k(\xi)$ . In fact, in the present context it is desirable to assume that  $x_k(\xi) \equiv 0$  for  $k = 1, \dots, 4$  since this guarantees that all the intermediate isoparametric (constant  $u$  and constant  $v$ ) curves meet the “boundary lines of curvature” orthogonally — i.e., in the complementary principal direction — and are thus (locally) also good approximations to lines of curvature.

Consistent with these choices, the departure/arrival vectors (32) may be expressed using cubics for  $y_1(\xi), \dots, y_4(\xi)$  as

$$\begin{aligned}\mathbf{T}_1(u) &= [\sigma_2(0) C_0(u) + a_{11} C_1(u) + a_{12} C_2(u) + \sigma_4(0) C_3(u)] \mathbf{h}_1(u), \\ \mathbf{T}_2(v) &= -[\sigma_1(0) C_0(v) + a_{21} C_1(v) + a_{22} C_2(v) + \sigma_3(0) C_3(v)] \mathbf{h}_2(v), \\ \mathbf{T}_3(u) &= [\sigma_2(1) C_0(u) + a_{31} C_1(u) + a_{32} C_2(u) + \sigma_4(1) C_3(u)] \mathbf{h}_3(u), \\ \mathbf{T}_4(v) &= -[\sigma_1(1) C_0(v) + a_{41} C_1(v) + a_{42} C_2(v) + \sigma_3(1) C_3(v)] \mathbf{h}_4(v),\end{aligned}\quad (42)$$

where  $\sigma_k(\xi) = |\mathbf{r}'_k(\xi)|$  for  $k = 1, \dots, 4$ .

### 4.3.2 Twist crossing constraints at corners

Consider, for example, the “twist constraint” (37) at the patch corner  $\mathbf{p}_{00}$ . From the Darboux relations (19), and using the fact that the geodesic torsion vanishes identically along lines of curvature, we have

$$\begin{aligned}\mathbf{T}'_1(0) &= \left. \frac{d}{du} \mathbf{T}_1(u) \right|_{u=0} = a_{11} \mathbf{h}_1(0) + \sigma_2(0) \mathbf{h}'_1(0) \\ &= a_{11} \mathbf{h}_1(0) + \sigma_2(0) [-\sigma_1(0) \kappa_{g,1}(0)] \mathbf{t}_1(0),\end{aligned}$$

where  $\kappa_{g,i}$  is the *geodesic curvature* of  $\mathbf{r}_i(\xi)$ . Similarly, we obtain

$$\mathbf{T}'_2(0) = \left. \frac{d}{dv} \mathbf{T}_2(v) \right|_{v=0} = -a_{21} \mathbf{h}_2(0) - \sigma_1(0) [-\sigma_2(0) \kappa_{g,2}(0)] \mathbf{t}_2(0).$$

Hence, from relations (31), we see that the parameters  $a_{11}$ ,  $a_{21}$  must be specified by

$$a_{11} = \sigma_1(0) \sigma_2(0) \kappa_{g,2}(0), \quad a_{21} = -\sigma_1(0) \sigma_2(0) \kappa_{g,1}(0)$$

in order for the twist constraint (37) to be satisfied at the corner  $\mathbf{p}_{00}$ , and the twist vector  $\mathbf{s}_{uv}(0,0)$  to be uniquely defined.

By considering analogous constraints at the other patch corners, so that the twist constraints (37–40) are satisfied, and the twist vectors  $\mathbf{s}_{uv}(i, j)$  are uniquely defined at each corner  $\mathbf{p}_{ij}$ , all the coefficients  $a_{kl}$  are determined if we use (42) as the departure/arrival vectors. Thus, with the cubic Coons scheme, no residual freedoms remain for smoothing the surface if it is not initially of good shape. As an alternative, a “pseudo–quintic” Coons scheme is described below, that provides a set of free parameters for surface smoothing.

#### 4.4 Pseudo–quintic Coons interpolant

As in the cubic case, we choose  $x_k(\xi) \equiv 0$ ,  $k = 1, \dots, 4$  in (32) to ensure that the isoparametric curves cross the patch boundaries orthogonally. Consider the four quintic polynomials  $A_0(\xi)$ ,  $A_1(\xi)$ ,  $A_4(\xi)$ ,  $A_5(\xi)$  specified on  $[0, 1]$  by

$$\begin{bmatrix} A_0(0) & A'_0(0) & A''_0(0) & A''_0(1) & A'_0(1) & A_0(1) \\ A_1(0) & A'_1(0) & A''_1(0) & A''_1(1) & A'_1(1) & A_1(1) \\ A_4(0) & A'_4(0) & A''_4(0) & A''_4(1) & A'_4(1) & A_4(1) \\ A_5(0) & A'_5(0) & A''_5(0) & A''_5(1) & A'_5(1) & A_5(1) \end{bmatrix} = \begin{bmatrix} 1 & 0 & \alpha_{01} & \alpha_{02} & 0 & 0 \\ 0 & 1 & \alpha_{11} & \alpha_{12} & 0 & 0 \\ 0 & 0 & \alpha_{41} & \alpha_{42} & 1 & 0 \\ 0 & 0 & \alpha_{51} & \alpha_{52} & 0 & 1 \end{bmatrix}$$

where  $\alpha_{ij}$  are free parameters. The first and last two columns of the matrix on the right indicate that these polynomials can replace the usual cubic Hermite basis in the bicubically blended Coons interpolation scheme. We also define the four polynomials  $B_0(\xi)$ ,  $B_1(\xi)$ ,  $B_4(\xi)$ ,  $B_5(\xi)$  in an analogous manner, but with free parameters  $\beta_{ij}$  in place of  $\alpha_{ij}$ . The interpolation scheme based on these polynomials is called “pseudo–quintic” because it does not use the true quintic Hermite basis (which permits  $C^2$  rather than just  $C^1$  interpolation).

Consider the three surfaces  $\mathbf{s}_{13}(u, v)$ ,  $\mathbf{s}_{24}(u, v)$ ,  $\mathbf{s}_0(u, v)$  defined by

$$\mathbf{s}_{13}(u, v) = [ B_0(v) \ B_1(v) \ B_4(v) \ B_5(v) ] \begin{bmatrix} \mathbf{r}_1(u) \\ \mathbf{T}_1(u) \\ \mathbf{T}_3(u) \\ \mathbf{r}_3(u) \end{bmatrix},$$

$$\mathbf{s}_{24}(u, v) = [ A_0(u) \ A_1(u) \ A_4(u) \ A_5(u) ] \begin{bmatrix} \mathbf{r}_2(v) \\ \mathbf{T}_2(v) \\ \mathbf{T}_4(v) \\ \mathbf{r}_4(v) \end{bmatrix},$$

$\mathbf{s}_0(u, v) =$

$$[A_0(u) A_1(u) A_4(u) A_5(u)] \begin{bmatrix} \mathbf{p}_{00} & \mathbf{r}'_2(0) & \mathbf{r}'_2(1) & \mathbf{p}_{01} \\ \mathbf{r}'_1(0) & \mathbf{s}_{uv}(0, 0) & \mathbf{s}_{uv}(0, 1) & \mathbf{r}'_3(0) \\ \mathbf{r}'_1(1) & \mathbf{s}_{uv}(1, 0) & \mathbf{s}_{uv}(1, 1) & \mathbf{r}'_3(1) \\ \mathbf{p}_{10} & \mathbf{r}'_4(0) & \mathbf{r}'_4(1) & \mathbf{p}_{11} \end{bmatrix} \begin{bmatrix} B_0(v) \\ B_1(v) \\ B_4(v) \\ B_5(v) \end{bmatrix}$$

where  $\alpha_{ij}, \beta_{ij}$  for  $i = 0, 1, 4, 5$  and  $j = 1, 2$  are free parameters. The desired interpolating surface is then defined by

$$\mathbf{s}(u, v) = \mathbf{s}_{13}(u, v) + \mathbf{s}_{24}(u, v) - \mathbf{s}_0(u, v). \quad (43)$$

#### 4.4.1 Departure & arrival vector fields

Choosing  $x_k(\xi) \equiv 0$  for  $k = 1, \dots, 4$  again, we use quintics for  $y_1(\xi), \dots, y_4(\xi)$  in (32). We then have

$$\begin{aligned} \mathbf{T}_1(u) &= [\sigma_2(0) Q_0(u) + a_{11} Q_1(u) + a_{12} Q_2(u) \\ &\quad + a_{13} Q_3(u) + a_{14} Q_4(u) + \sigma_4(0) Q_5(u)] \mathbf{h}_1(u), \\ \mathbf{T}_2(v) &= -[\sigma_1(0) Q_0(v) + a_{21} Q_1(v) + a_{22} Q_2(v) \\ &\quad + a_{23} Q_3(v) + a_{24} Q_4(v) + \sigma_3(0) Q_5(v)] \mathbf{h}_2(v), \\ \mathbf{T}_3(u) &= [\sigma_2(1) Q_0(u) + a_{31} Q_1(u) + a_{32} Q_2(u) \\ &\quad + a_{33} Q_3(u) + a_{34} Q_4(u) + \sigma_4(1) Q_5(u)] \mathbf{h}_3(u), \\ \mathbf{T}_4(v) &= -[\sigma_1(1) Q_0(v) + a_{41} Q_1(v) + a_{42} Q_2(v) \\ &\quad + a_{43} Q_3(v) + a_{44} Q_4(v) + \sigma_3(1) Q_5(v)] \mathbf{h}_4(v), \end{aligned} \quad (44)$$

$Q_0(\xi), \dots, Q_5(\xi)$  being the quintic Hermite basis functions (see Appendix). In this case, eight of the coefficients  $a_{ij}$  remain as free parameters for surface smoothing after specification of the corner twist vectors below.

#### 4.4.2 Twist crossing constraints at corners

Consider the twist constraint (37) at the patch corner  $\mathbf{p}_{00}$ . From the Darboux relations (19), and using the fact that the geodesic torsion vanishes identically along lines of curvature, we have

$$\begin{aligned} \mathbf{T}'_1(0) &= \left. \frac{d}{du} \mathbf{T}_1(u) \right|_{u=0} = a_{11} \mathbf{h}_1(0) + \sigma_2(0) \mathbf{h}'_1(0) \\ &= a_{11} \mathbf{h}_1(0) + \sigma_2(0) [-\sigma_1(0) \kappa_{g,1}(0)] \mathbf{t}_1(0), \end{aligned}$$

where  $\kappa_{\mathbf{g},i}$  is the *geodesic curvature* of  $\mathbf{r}_i(\xi)$ . Similarly, we obtain

$$\mathbf{T}'_2(0) = \left. \frac{d}{dv} \mathbf{T}_2(v) \right|_{v=0} = -a_{21} \mathbf{h}_2(0) - \sigma_1(0) \left[ -\sigma_2(0) \kappa_{\mathbf{g},2}(0) \right] \mathbf{t}_2(0).$$

Hence, from relations (31), we see that the parameters  $a_{11}$ ,  $a_{21}$  must be specified by

$$a_{11} = \sigma_1(0) \sigma_2(0) \kappa_{\mathbf{g},2}(0), \quad a_{21} = -\sigma_1(0) \sigma_2(0) \kappa_{\mathbf{g},1}(0)$$

in order for the twist constraint (37) to be satisfied at the corner  $\mathbf{p}_{00}$ , and the twist vector  $\mathbf{s}_{uv}(0,0)$  to be uniquely defined. By considering the analogous constraints at the other corners, the twist constraints (37–40) are satisfied, and the twist vectors  $\mathbf{s}_{uv}(i,j)$  are uniquely defined at each corner  $\mathbf{p}_{ij}$ .

Note that, in the above surface construction process, the eight coefficients  $a_{k2}$ ,  $a_{k3}$  for  $k = 1, \dots, 4$  and the 16 quantities  $\alpha_{ij}$ ,  $\beta_{ij}$  for  $i = 0, 1, 4, 5$  and  $j = 1, 2$  remain as free parameters for the surface smoothing process.

**Remark 1.** By inspection of the above interpolation processes, one can easily verify that  $\mathbf{s}(u,v)$  defined by (41) or (43) is a rational surface.

Another way to obtain surface smoothing parameters is to assume non-zero polynomials  $x_k(\xi)$  in the departure/arrival vectors (32). As noted above, however, we consider this approach less desirable, since the orthogonality of the intermediate isoparametric curves to the patch boundaries makes them good (local) approximations to the surface lines of curvature.

## 5 Computed examples

**Example 1.** As the patch corner points  $\mathbf{p}_{ij}$  and associated frames  $(\mathbf{t}_{ij}, \mathbf{h}_{ij}, \mathbf{n}_{ij})$  for  $i, j = 0, 1$  we take

$$\mathbf{p}_{00} = (0, 0, 0), \quad \mathbf{p}_{10} = (1, 0, 0), \quad \mathbf{p}_{01} = (0, 1, 0), \quad \mathbf{p}_{11} = (1, 1, 0),$$

$$\begin{aligned}
\mathbf{t}_{00} &= (0.951392, -0.306558, -0.029597), \\
\mathbf{h}_{00} &= (0.307228, 0.951392, 0.021552), \\
\mathbf{n}_{00} &= (0.021552, -0.029597, 0.999330), \\
\mathbf{t}_{10} &= (0.960566, 0.276802, 0.026353), \\
\mathbf{h}_{10} &= (-0.277346, 0.960566, 0.019826), \\
\mathbf{n}_{10} &= (-0.019826, -0.026353, 0.999456), \\
\mathbf{t}_{01} &= (0.930257, 0.365113, -0.036238), \\
\mathbf{h}_{01} &= (-0.366075, 0.930257, -0.024694), \\
\mathbf{n}_{01} &= (0.024694, 0.036238, 0.999038), \\
\mathbf{t}_{11} &= (0.982409, -0.185972, 0.016964), \\
\mathbf{h}_{11} &= (0.186215, 0.982409, -0.014052), \\
\mathbf{n}_{11} &= (-0.014052, 0.016964, 0.999757).
\end{aligned}$$

This initial data is shown in Figure 2, together with the four quintic RRMF boundary curves that interpolate it. Figure 3 shows the unit surface normals and tangent normals (i.e., the normal components of the rotation–minimizing frames) associated with these curves — these are exactly specified as rational vector fields in the curve parameters, in the degree 8 Bernstein basis.

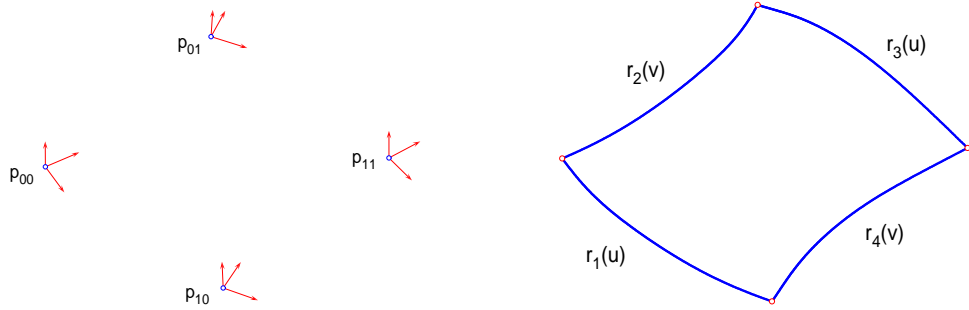


Figure 2: Left: surface patch corner points and associated frames, defining the principal directions and surface normal. Right: interpolation of the patch corner data by four quintic RRMF curves, that define the patch boundaries.

In this case, a smooth surface was obtained using the simple cubic Coons interpolation scheme described in Section 4.3 — there is no need to introduce additional free parameters (see Section 4.4) for surface smoothing purposes. Figure 4 shows the resulting rational surface patch.

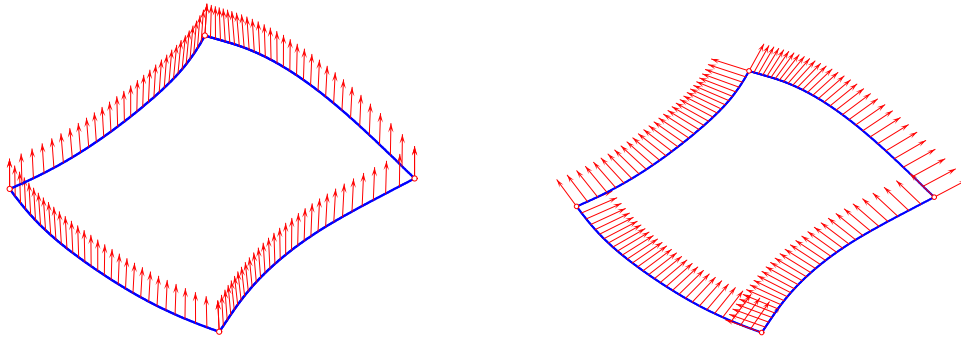


Figure 3: Variation of the surface normal  $\mathbf{n}$  (left) and the tangent normal  $\mathbf{h}$  (right) along the surface patch boundaries. Together with the curve tangent  $\mathbf{t}$ , these vectors define the Darboux frame  $(\mathbf{t}, \mathbf{h}, \mathbf{n})$  along each boundary, and by construction the vectors  $\mathbf{h}, \mathbf{n}$  are rotation-minimizing with respect to  $\mathbf{t}$ .

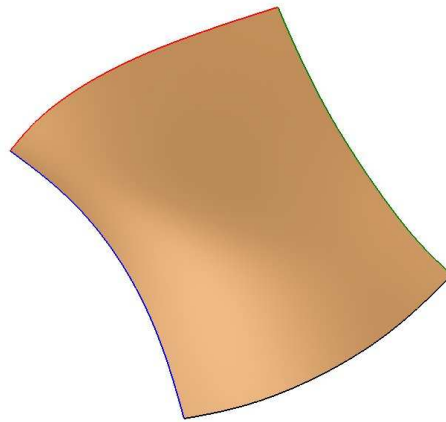


Figure 4: The rational surface patch bounded by lines of curvature (quintic RRMF curves) generated from the boundary data shown in Figures 2 and 3.

**Example 2.** Figures 5 and 6 show two more examples, using the same corner points as in Example 1 but different frames to specify the surface normal and principal directions at those corner points. In these cases, the initial surfaces obtained with the cubic Coons scheme of Section 4.3 were of unsatisfactory shape, so the pseudo–quintic Coons scheme of Section 4.4 was used instead. The figures show the surfaces before and after minimization of the thin–plate spline energy with respect to the free parameters introduced in Section 4.4.

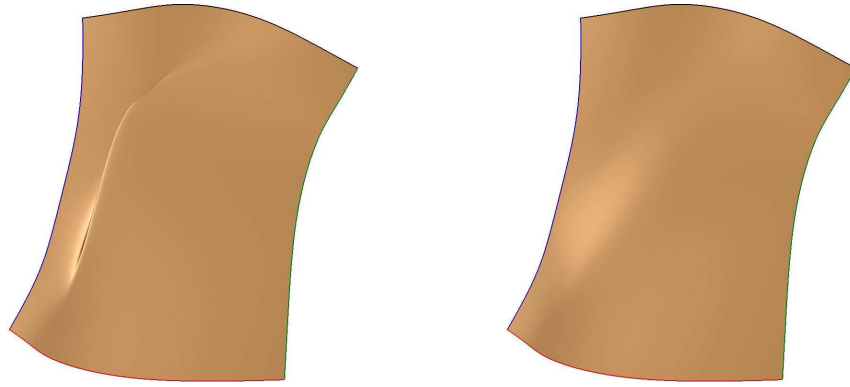


Figure 5: Left: rational surface patch bounded by lines of curvature before smoothing. Right: the same surface patch after minimization of thin–plate spline energy with respect to the free parameters described in Section 4.4.

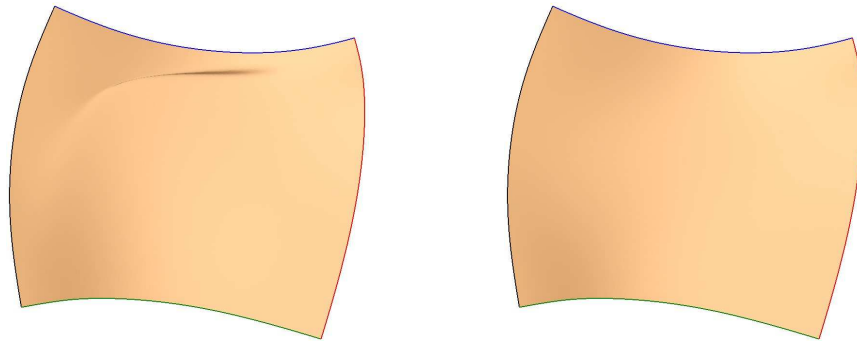


Figure 6: Left: rational surface patch bounded by lines of curvature before smoothing. Right: the same surface patch after minimization of thin–plate spline energy with respect to the free parameters described in Section 4.4.

## 6 Closure

A method for creating rational surface patches bounded by lines of curvature has been developed, based on a Coons interpolation scheme. The initial data comprises a set of patch corner points with associated orthonormal frames, that define the surface normal and principal curvature directions. The patch boundary curves are then defined as quintic PH curves with rational rotation–minimizing frames (quintic RRMF curves). Since the surface Darboux frame is rotation–minimizing (with respect to the tangent) along lines of curvature, Coons interpolation of these RRMF boundary curves and associated frames ensures that they are lines of curvature on the constructed surface.

Another notable feature of the construction is that the transverse surface isoparametric curves are orthogonal to the line–of–curvature boundaries, and are thus also excellent (local) approximations to lines of curvature. Although the resulting rational surface patches are of relatively high degree, this is not problematic if the construction is systematically executed in the numerically–stable Bernstein form. It can be expected that the proposed scheme will prove useful when surfaces are to be designed with precise control over curvature properties — e.g., by the interpolation of prescribed “feature” lines.

The intent of this paper has been to demonstrate the feasibility and basic methodology for the construction of rational surface patches bounded by lines of curvature, and a number of technical issues must be further addressed to facilitate the development of a robust surface design system. These include extending known solutions of the geometric Hermite interpolation problem using RRMF curves, to ensure existence of interpolants to general data, and the incorporation and utilization of free smoothing parameters in the Coons scheme, to produce surfaces of optimum shape quality.

## Appendix: Hermite basis functions

The cubic and quintic Hermite bases on the interval  $\xi \in [0, 1]$  are employed in the Coons interpolation scheme. The cubic basis functions, defined by

$$\begin{aligned} C_0(\xi) &= 1 - 3\xi^2 + 2\xi^3, \\ C_1(\xi) &= \xi - 2\xi^2 + \xi^3, \\ C_2(\xi) &= -\xi^2 + \xi^3, \\ C_3(\xi) &= 3\xi^2 - 2\xi^3, \end{aligned}$$

satisfy the boundary conditions

$$\begin{bmatrix} C_0(0) & C'_0(0) & C''_0(1) & C_0(1) \\ C_1(0) & C'_1(0) & C''_1(1) & C_1(1) \\ C_2(0) & C'_2(0) & C''_2(1) & C_2(1) \\ C_3(0) & C'_3(0) & C''_3(1) & C_3(1) \end{bmatrix} = \begin{bmatrix} 1 & 0 & 0 & 0 \\ 0 & 1 & 0 & 0 \\ 0 & 0 & 1 & 0 \\ 0 & 0 & 0 & 1 \end{bmatrix},$$

Similarly, the quintic basis functions are defined by

$$\begin{aligned} Q_0(\xi) &= -6\xi^5 + 15\xi^4 - 10\xi^3 + 1, \\ Q_1(\xi) &= -3\xi^5 + 8\xi^4 - 6\xi^3 + \xi, \\ Q_2(\xi) &= \frac{1}{2}(-\xi^5 + 3\xi^4 - 3\xi^3 + \xi^2), \\ Q_3(\xi) &= \frac{1}{2}(\xi^5 - 2\xi^4 + \xi^3), \\ Q_4(\xi) &= -3\xi^5 + 7\xi^4 - 4\xi^3, \\ Q_5(\xi) &= 6\xi^5 - 15\xi^4 + 10\xi^3, \end{aligned}$$

and satisfy

$$\begin{bmatrix} Q_0(0) & Q'_0(0) & Q''_0(0) & Q''_0(1) & Q'_0(1) & Q_0(1) \\ Q_1(0) & Q'_1(0) & Q''_1(0) & Q''_1(1) & Q'_1(1) & Q_1(1) \\ Q_2(0) & Q'_2(0) & Q''_2(0) & Q''_2(1) & Q'_2(1) & Q_2(1) \\ Q_3(0) & Q'_3(0) & Q''_3(0) & Q''_3(1) & Q'_3(1) & Q_3(1) \\ Q_4(0) & Q'_4(0) & Q''_4(0) & Q''_4(1) & Q'_4(1) & Q_4(1) \\ Q_5(0) & Q'_5(0) & Q''_5(0) & Q''_5(1) & Q'_5(1) & Q_5(1) \end{bmatrix} = \begin{bmatrix} 1 & 0 & 0 & 0 & 0 & 0 \\ 0 & 1 & 0 & 0 & 0 & 0 \\ 0 & 0 & 1 & 0 & 0 & 0 \\ 0 & 0 & 0 & 1 & 0 & 0 \\ 0 & 0 & 0 & 0 & 1 & 0 \\ 0 & 0 & 0 & 0 & 0 & 1 \end{bmatrix}.$$

## References

- [1] R. L. Bishop (1975), There is more than one way to frame a curve, *Amer. Math. Monthly* **82**, 246–251.
- [2] H. I. Choi and C. Y. Han (2002), Euler–Rodrigues frames on spatial Pythagorean–hodograph curves, *Comput. Aided Geom. Design* **19**, 603–620.
- [3] H. I. Choi, D. S. Lee, and H. P. Moon (2002), Clifford algebra, spin representation, and rational parameterization of curves and surfaces, *Adv. Comp. Math.* **17**, 5–48.

- [4] S. Coons (1964), Surfaces for Computer Aided Design, Technical Report, M.I.T., (available as AD 663 504 from National Technical Information Service, Springfield, VA 22161)
- [5] S. Coons (1974), Surface patches and B-spline curves, in *Computer Aided Geometric Design* (R. Barnhill and R. Riesenfeld, eds.), Academic Press.
- [6] R. Dietz, J. Hoschek, and B. Jüttler (1993), An algebraic approach to curves and surfaces on the sphere and on other quadrics, *Comput. Aided Geom. Design* **10**, 211–229.
- [7] G. Farin (2002), *Curves and Surfaces for CAGD* (5th Edition), Academic Press, 2002
- [8] R. T. Farouki (1998), On integrating lines of curvature, *Comput. Aided Geom. Design* **15**, 187–192.
- [9] R. T. Farouki (2002), Exact rotation–minimizing frames for spatial Pythagorean–hodograph curves, *Graph. Models* **64**, 382–395.
- [10] R. T. Farouki (2008), *Pythagorean–Hodograph Curves: Algebra and Geometry Inseparable*, Springer, Berlin.
- [11] R. T. Farouki (2009), Quaternion and Hopf map characterizations for the existence of rational rotation–minimizing frames on quintic space curves, *Adv. Comp. Math.* to appear.
- [12] R. T. Farouki, M. al–Kandari, and T. Sakkalis (2002), Hermite interpolation by rotation–invariant spatial Pythagorean–hodograph curves, *Adv. Comp. Math.* **17**, 369–383.
- [13] R. T. Farouki, C. Giannelli, C. Manni, and A. Sestini (2008), Identification of spatial PH quintic Hermite interpolants with near–optimal shape measures, *Comput. Aided Geom. Design* **25**, 274–297.
- [14] R. T. Farouki, C. Giannelli, C. Manni, and A. Sestini (2009), Quintic space curves with rational rotation–minimizing frames, *Comput. Aided Geom. Design* **26**, 580–592.

- [15] R. T. Farouki, C. Giannelli, C. Manni, and A. Sestini (2009), Hermite interpolation by quintic space curves with rational rotation–minimizing frames, and applications to rigid body motion specification, preprint.
- [16] R. T. Farouki, C. Giannelli, and A. Sestini (2009), Geometric design using space curves with rational rotation–minimizing frames, to appear.
- [17] R. T. Farouki and C. Y. Han (2003), Rational approximation schemes for rotation–minimizing frames on Pythagorean–hodograph curves, *Comput. Aided Geom. Design* **20**, 435–454.
- [18] R. T. Farouki, N. Szafran, and L. Biard (2009), Existence conditions for Coons patches interpolating geodesic boundary curves, *Comput. Aided Geom. Design* **26**, 599–614.
- [19] R. T. Farouki, N. Szafran, and L. Biard (2009), Construction of Bézier surface patches with Bézier curves as geodesic boundaries, *Comput. Aided Design* **41**, 772–781.
- [20] C. Y. Han (2008), Nonexistence of rational rotation–minimizing frames on cubic curves, *Comput. Aided Geom. Design* **25**, 298–304.
- [21] W. Gordon (1983), An operator calculus for surface and volume modeling, *IEEE Comput. Graph. Appl.* **3**, 18–22.
- [22] H. Guggenheimer (1989), Computing frames along a trajectory, *Comput. Aided Geom. Design* **6**, 77–78.
- [23] B. Jüttler (1998), Generating rational frames of space curves via Hermite interpolation with Pythagorean hodograph cubic splines, in *Geometric Modeling and Processing '98*, Bookplus Press, pp. 83–106.
- [24] B. Jüttler and C. Mäurer (1999), Cubic Pythagorean hodograph spline curves and applications to sweep surface modelling, *Comput. Aided Design* **31**, 73–83.
- [25] B. Jüttler and C. Mäurer (1999), Rational approximation of rotation minimizing frames using Pythagorean–hodograph cubics, *J. Geom. Graphics* **3**, 141–159.

- [26] F. Klok (1986), Two moving coordinate frames for sweeping along a 3D trajectory, *Comput. Aided Geom. Design* **3**, 217–229.
- [27] E. Kreyszig (1959), *Differential Geometry*, University of Toronto Press.
- [28] R. R. Martin (1982), Principal Patches for Computational Geometry, PhD Thesis, Cambridge University.
- [29] J. Roe (1993), *Elementary Geometry*, Oxford University Press.
- [30] D. J. Struik (1988), *Lectures on Classical Differential Geometry*, Dover Publications (reprint), New York.
- [31] W. Wang and B. Joe (1997), Robust computation of the rotation minimizing frame for sweep surface modelling, *Comput. Aided Design* **29**, 379–391.
- [32] W. Wang, B. Jüttler, D. Zheng, Y. Liu (2008), Computation of rotation minimizing frames, *ACM Trans. Graphics* **27**, No. 1, Article 2, 1–18.